THESIS FOR THE DEGREE OF LICENTIATE OF ENGINEERING

Development of a new generation of 12% chromium steels:

Z-phase strengthened steels

Masoud Rashidi

Department of Applied Physics

CHALMERS UNIVERSITY OF TECHNOLOGY

Gothenburg, Sweden 2015

Development of a new generation of 12% chromium steels: Z-phase strengthened steels

Department of Applied Physics
Chalmers University of Technology
SE-412 96 Gothenburg
Sweden
Telephone: +46 (0)31-772 3337

Printed by:
Chalmers Reproservice
Gothenburg Sweden 2015
Development of a new generation of 12% chromium steels: Z-phase strengthened steels

Masoud Rashidi
Department of Applied Physics
Chalmers University of Technology

Abstract

Fossil-fuel fired steam power plants provide more than 60% of the electricity generated worldwide, and account for about one third of the global CO_2 emissions. The thermal efficiency of the steam power plants is limited by the maximum allowed steam temperature and pressure, which in turn are determined by the long-term corrosion and creep resistance of economically viable materials. Today's best martensitic steels contain 9% Cr and can be used at ~ 600°C/300 bar. All attempts so far to reach 650°C with 11-12% Cr steels have failed, and the reason is the formation of a complex nitride, Z-phase, after a few years of service.

In this thesis it is shown that Z-phase can be used as strengthening rather than weakening phase to develop a new generation of martensitic steels. These steels contain 12% Cr for better corrosion resistance and densely distributed fine Z-phase precipitates for creep resistance. A high Cr content together with Ta and N additions were used to stimulate the formation of a fine distribution of Z-phase in two trial steels. Atom probe tomography, transmission electron microscopy, and scanning electron microscopy were employed for a detailed characterization of the microstructure.

In the first trial steel, 12Cr7CoTa-uLC, the C content was limited to 0.005 wt.%, which resulted in a fast transformation from TaN to CrTaN Z-phase, and subsequently a fine distribution of Z-phase was achieved. In the second trial steel, 12Cr3CoTa-HC, a higher C content of 0.06 wt.% was used, which resulted in a slower phase transformation from Ta(C,N) to CrTaN Z-phase.

In the 12Cr7CoTa-uLC trial steel Laves phase formed continuously at the prior austenite grain boundaries, which gave poor impact toughness. In the second trial steel, the addition of Cu and a higher C content improved the distribution of Laves phase, and equiaxed Laves phase particles of a few hundred nanometer in size formed resulting in improved toughness.

Keywords: martensitic steels, creep, Z-phase, precipitation hardening, 9-12% Cr steels, transmission electron microscopy, atom probe tomography

Preface

The research work presented in this thesis was carried out in the Division of Materials Microstructure at the Department of Applied Physics, Chalmers University of Technology, Gothenburg, Sweden, during the period May 2013 to September 2015, under supervision of Assistant Professor Fang Liu and Professor Hans-Olof Andrén.

This project has been performed within the framework of the Swedish consortium for materials technology in thermal energy processes, KME (contract number: 510 and 710), the Swedish Energy Agency (contract number 31139-1), the Research Foundation of VGB (contract number: 348), and within the Z-ultra project, which received funding from the European Union's Seventh Framework Program for research, technological development, and demonstration under grant agreement No. 309916.

The following papers are included in this thesis:

I. F Liu, M Rashidi, L Johansson, J Hald, H-O Andrén, "A new 12% chromium steel strengthened by Z-phase precipitates" submitted to Scripta Materiala.

II. M Rashidi, F Liu, H-O Andrén, "Microstructure characterization of two Z-phase strengthened 12% chromium steels" in Proc. 10th Liège Conference: Materials for Advanced Power Engineering 2014, Eds. J Lecomte-Beckers, O Dedry, J Oakey and B Kuhn, pp. 71-80. (electronic form only)

*Difficulties strengthen the mind, as **particles** do the **steel**!*

Masoud

(Inspired by Lucius Annaeus Seneca
Roman Philosopher)

Table of Contents

1. Introduction

Energy security and environmental protection are regarded as extremely essential issues throughout the world. One of the most effective ways to reduce the CO_2 emission is to limit the fossil fuel consumption. Fossil-fired power plants account for about one third of the global CO_2 emissions [1]. Therefore, enhancing the energy conversion efficiency and thereby reducing the CO_2 emissions in new steam power plants, mainly through increasing operating steam temperature and pressure, is considered as one of the solutions for the next few decades. However, the efficiency is often limited by the availability of economically viable structural materials with good long-term corrosion and creep resistance against the increased temperature and pressure. The required lifetime of the materials is 200,000 hours, which is more than 22 years. Martensitic 9-12% Cr steels offer an optimal combination of the critical properties, i.e. creep strength, corrosion resistance, thermal conductivity and thermal expansion, at a relatively low cost. Therefore, they are by far the most used material for steam pipes and turbine components. The development of ultra supercritical power plants started in the 1980s and since then progressive increases in steam temperature and pressure have been achieved, and now power plants with steam temperatures ranging from 590-610°C have been successfully built [2].

This thesis studies the feasibility of a new generation of creep resistant high Cr martensitic/ferritic steels, Z-phase strengthened 12% chromium steels, which are believed to be capable of combining good corrosion and creep properties at a steam temperature of 650°C.

1.1 Application and motivations for alloy development

Tempered martensitic 9-12% Cr steels have successfully been used in fossil-fired steam power plants mainly in thick components such as steam pipes, headers, steam chests, valve bodies, turbine housings, etc.

In thermal power plants, water is used as the working fluid. A boiler is used to produce hot steam. This high pressure and high temperature steam then rotates the blades of a turbine and thus produces electricity through a generator. The higher the steam temperature and pressure, the higher thermal efficiency is achieved. According to the Carnot cycle, the efficiency of steam power plants is affected by steam temperature. The efficiency η is calculated to be:

$$\eta = 1 - \frac{T_C}{T_H}$$

where T_C is the absolute temperature of the condensed water and T_H is the absolute temperature of the steam. However, the Carnot cycle cannot be reached practically due to some limitations and it is worth mentioning that in practice, the Rankine cycle with reheating is used in steam power plants. Ultra-super critical (USC) power plants are operated above the critical point of water, i.e. 374°C and 220 bar.

Considering the fact that fossil-fired steam power plants produce more than 60% of world's electricity [1], there is always an interest in increasing the thermal efficiency

of power plants to minimize the fuel consumption and CO_2 emissions. Developing creep resistant steels that can be used at higher steam temperatures and pressures for longer times is the key to increase thermal efficiency. These extreme conditions of high temperatures and steam pressure will worsen classic high temperature material problems such as microstructural degradation, creep, oxidation, corrosion, and fatigue. Low chromium steels and 9% Cr steels, which have been used to a large extent for steam turbines, do not provide proper creep and corrosion resistance for the higher steam temperature of 650°C. Thus, there is a need for better materials to withstand such extreme conditions.

In the power plants with frequent stop and start cycles or in the ones capable of responding to changes in the electricity demand and accommodating the fluctuations from renewable energies, thermal stress and thermal fatigue needs to be minimized. Poor thermal conductivity and high thermal expansion coefficient are the main reasons for not using austenitic steels for such applications since they will suffer from thermal fatigue.

Optimized creep resistant 9-12 % Cr steels with small coefficient of thermal expansion (provides more structural stability) and better thermal conductivity (provides better heat transfer rates when the temperature of the component changes) are believed to be the right material to be used for further improvement in the efficiency of the steam power plants. Furthermore, ferritic steels have lower amounts of expensive elements and are thus cheaper compared to the austenitic ones [3], [4].

1.2 Scope of this work

This research was undertaken in order to evaluate the feasibility of using precipitates of a thermodynamically stable phase, Z-phase, as strengthening agent to achieve proper creep strength at a steam temperature of 650°C. Moreover, the role of other precipitates on the mechanical properties of Z-phase strengthened steels was also studied.

The work is done in close collaboration with the Technical University of Denmark, Siemens Industrial Turbomachinery AB, Fraunhofer IWM Freiburg, Saarschmiede GmbH, Graz University of Technology, and E.O. Paton Electric Welding Institute. The work at Chalmers was mainly to study the microstructure of trial steels in the as-tempered condition, and after ageing for different times.

2. Background

2.1 Iron and steel

Iron has a body-centered cubic (bcc) structure (α-iron or ferrite) at room temperature and this structure is stable up to 910°C. In the temperature range of 910°C to 1390°C, iron has a face-centered cubic (fcc) structure, which is called γ-iron or austenite. Above 1390°C, iron returns to bcc structure and forms δ-ferrite, which is stable up to the melting temperature of 1536°C, see Figure 2.1. These changes in structure are very important and affect the physical and mechanical properties of the material.

Iron alloys with less than 2 wt.% C are generally classified as steel. Low carbon steels contain up to 0.3 wt.% C. Medium carbon steels contain 0.3 to 0.8 wt.% C and steels with higher carbon content are classified as high carbon steels. Steels are often the "gold standard" against other structural materials. Thanks to the regular and exciting discoveries in the context of iron and its alloys, steels remain as the most successful and cost-effective of all materials. Steels help improving the quality of our everyday life with the consumption of more than a billion tonnes per year. One reason for such a high consumption of steels is the endless variety of properties and microstructure that can be achieved by altering composition and processing parameters.

Among all different grades of steels, high chromium steels have successfully been used in different parts of fossil-fired steam power plants. 9-12% Cr steels capable of operating in ultra supercritical power plants are the alloys of interest in this thesis.

2.2 Creep

Creep is a slow and continuous plastic deformation of materials under mechanical stress for a prolonged period of time. Creep can occur at any temperatures above zero Kelvin, however it is traditionally associated with time-dependent plastic deformation of a material at elevated temperatures often higher than $0.4T_m$ (T_m is absolute melting temperature of the material) under a mechanical stress below the yield stress of the material.

For steels, creep tests are mostly done at a constant load and temperature. The obtained results from tests are presented as creep curves, which graphically represent the time-dependence of strain. In Figure 2.2, three stages of creep, primary or transient creep, secondary or steady-state creep, and tertiary or accelerated creep, are schematically shown.

The instantaneous strain, ε_0 is a combination of elastic strain and possible plastic strain depending on the tensile stress level. In the region between ε_0 and ε_1, primary creep region, creep rate decreases with time due to strain hardening or a decrease in free or mobile dislocations. Between ε_1 and ε_2, the creep rate remains constant and a steady-state creep rate is achieved mainly due to a balance between generation and recovery of dislocations. In the tertiary creep stage, the creep rate increases with time until rupture. Necking of the specimen and formation of cavities reduce the cross-section and thus increase the stress under constant load. The increase in the creep rate can also be attributed to the microstructure evolution during creep. The microstructure evolution during creep mainly consists of dynamic recovery, dynamic recrystallization, and coarsening of precipitates.

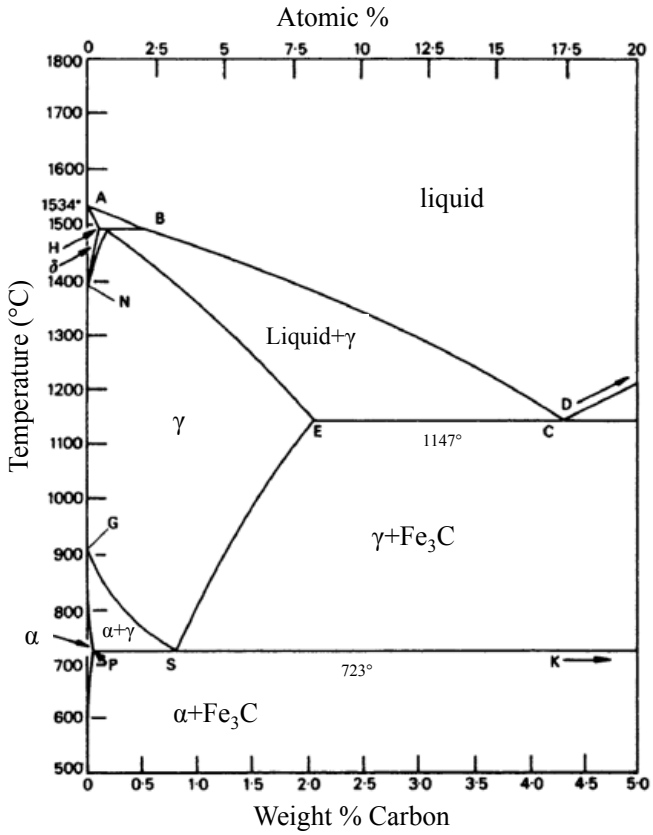

Figure 2.1. The Iron-carbon phase diagram [5].

In Figure 2.2, the idealized creep and creep rate curves are shown. However, creep-resistant steels might exhibit a different creep behavior. For example, under certain conditions, the steady-state stage might be absent and after the transient creep stage, the accelerated creep starts. It is believed that there is an ever-evolving microstructure during creep so that dynamic microstructural equilibrium cannot be reached in creep-resistant steels and thus a minimum creep rate is introduced instead of the steady-state creep stage.

Another complicated creep behavior occurs in some special steels under low stress and long-time conditions, which is mainly due to the microstructural evolution during creep such as precipitation of a new phase or coarsening of particles after an extended period. The creep rupture data are usually presented in a graph showing the relationship between σ, applied stress, and t_r, time to rupture.

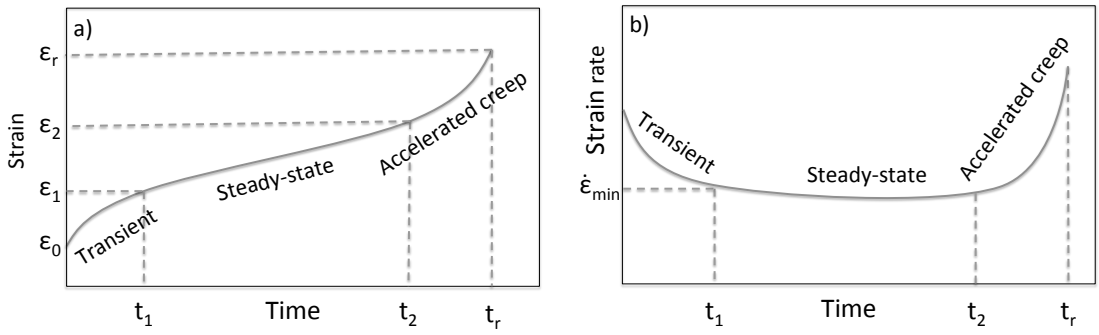

Figure 2.2. Schematic a) creep curve and b) creep rate curve under constant tensile load and constant temperature.

2.3 Strengthening mechanisms

The strengthening mechanisms in creep-resistant steels with an emphasis on tempered martensitic 9-12% Cr steels are briefly described. The four strengthening mechanisms for creep-resistant steels are solid solution hardening, precipitation hardening, dislocation hardening, and boundary hardening. In creep-resistant steels, a combination of strengthening mechanisms provides the creep strength at elevated temperatures. The reader is advised to read reference [6] for more details.

Solid solution hardening

Substitutional solute atoms with a larger atomic size compared to the solvent iron, e.g Mo and W, are effective solid solution strengtheners in both ferritic and austenitic steels. By considering the Hume-Rothery size effect and large solubility in iron, Ir and Re can also provide proper solid solution strengthening. It is also well known that in case of interstitial solute atoms, nitrogen is beneficial for long term creep resistance through both solid solution hardening and precipitation hardening.

Precipitation hardening

Precipitation hardening is one of the important strengthening mechanisms in creep-resistant steels and especially in 9-12% Cr steels at elevated temperatures. To provide sufficient strengthening through precipitates, usually different kinds of precipitates are located inside the matrix or at the boundaries such as, $M_{23}C_6$, M_6C, M_7C_3, MX, and M_2X (M stands for the metallic element, and X is carbon and/or nitrogen), intermetallic compounds such as Fe_2(Mo, W) Laves phase, and metallic phases, such as Cu. A fine distribution of precipitates enhances the dislocation hardening and boundary hardening by stabilizing the free dislocation in the matrix and sub-grain structure [7].

Several mechanisms have been proposed to calculate the stress needed for a dislocation to pass a precipitate particle. These mechanisms are Orowan mechanism, local and general climb mechanism, and Srolovitz mechanism, which are explained in details in reference [6].

According to the Orowan mechanism, the stress required for a dislocation to pass a precipitate particle is calculated through the following equation:

$\sigma_{Or} = 0.8\ MGb/\lambda$

Where M is Taylor factor (=3), G is the shear modulus, b is the Burgers vector, and λ is the average interparticle distance. The interparticle distance is related to the volume fraction and the mean size of the particles. In 9-12% Cr steels, λ increases by coarsening $M_{23}C_6$, Laves phase, and MX, or dissolution of MX to form massive Z-phase particles. Increasing the λ results in weakening the material over long periods of time. Coarsening or dissolution of fine particles near grain boundaries results in localized weak zones and promotes premature creep rupture due to localized creep deformation. The technically interesting stress and temperature ranges for 9-12% Cr steels during service exposure and creep testing are 20 MPa to 250 MPa and 700 °C to 500 °C. In these ranges, dislocation creep is the main creep mechanism, which leads to glide and climb of free dislocations and movement of sub-boundaries. Precipitation hardening is mainly employed to delay the deformation process by pinning dislocations and sub-boundaries [8]–[10].

Dislocation hardening

Dislocation hardening is an important strengthening mechanism at room temperature. The higher the dislocation density, the higher strength is achieved by dislocation hardening. In 9-12% Cr steels, a high density of dislocations is achieved after quenching and it remains even after tempering. Normally the tempering temperature is defined based on the application, for example, in turbine steels tempering is done at low temperatures of 700°C to ensure sufficient tensile strength at ambient temperature by dislocation hardening while the tempering temperatures normally are in the range of 750°C-800°C for boiler applications [10].

However, at elevated temperature, these excess dislocations accelerate recovery and recrystallization of deformed microstructure during creep. High temperature tempering results in lower density of dislocation and thus increases the creep life of the alloy compared to lower temperature tempering, where the density of excess dislocation is too high and accelerates the recovery and recrystallization of the deformed microstructure.

Sub-boundary hardening

After austenitization and tempering 9-12% Cr steels show a lath martensitic microstructure consisting of laths and blocks with a high density of dislocations and a dispersion of precipitates along the lath and block boundaries. These lath and block boundaries provide the sub-boundary hardening, which is given by:

$\sigma_{sg} = 10\ Gb/\ \lambda_{sg}$

Where λ_{sg} is the short width of the elongated lath and block boundaries in the range of few hundreds of nm in the tempered martensitic 9-12% Cr steels.

The mobile nature of lath and block boundaries mainly in the accelerated creep region results in increasing the λ_{sg}. The movement of these boundaries absorbs the excess dislocations and results in softening through a dynamic recovery process.

The fine distribution of $M_{23}C_6$ and MX precipitates along the boundaries stabilizes the boundaries and provides a pinning force against the movement of boundaries and thus retards the increase in the λ_{sg} during creep. Thus, particle-stabilized substructure hardening is the most important mechanism in 9-12% Cr steels to obtain long-term creep resistance [10], [11].

3. 9-12% Cr steels

The purpose of this chapter is to provide a brief overview of the 9-12% Cr steels including historical developments, physical metallurgy, microstructure and microstructural evolution during creep.

3.1 Historical developments

Up to 1920s, carbon steels were generally used for components in the steam power plants. These steels were exposed to a maximum temperature of 350°C at a pressure of 15 bar. Low-alloyed steels were introduced in the beginning of 1920s and thus the operating temperature in the power plants was increased to 450°C with the pressure of 35 bar. Until 1950s, some alloying elements such as Mo, Mn, Si, Cr, and V were added to the steels to improve their high temperature strength and corrosion resistance.

The first leap for developing 9-12% Cr steels was in 1950s, when the development of thermal power plants operating at a steam temperature of 538°C-566°C for public power supply began. The second leap was in 1980s when the goal was to develop low-pollution power plants operating at higher steam temperatures of 600°C-650°C and supercritical pressures up to 350 bar. Since 1980s, many national and international research projects have been in progress in Japan, USA, and Europe [12].

At steam temperatures of 600°C, tempered martensitic 9-12% Cr steels are more favorable compared to low chromium steels due to their higher creep strength as well as their better oxidation resistance.

3.1.1 Achievements

X22CrMoV, containing 12% Cr and 1% Mo, is one of the early tempered martensite ferritic steels that was developed in Germany in the 1950s. Its creep strength is based on solid solution hardening and precipitation of $M_{23}C_6$ carbides.

Adding Nb and N into steels, for example H64 (UK), FV448 (UK), and 56TS (France), resulted in further increase in strength by precipitation of secondary MX particles of type VN and Nb(C,N). Boron was recognized as a beneficial element for improving creep strength by stabilizing $M_{23}(C,B)_6$, for example the TAF steel (Japan).

The steel 9Cr1MoV or the so-called P91 steel was developed in USA in the late 1970s originally to manufacture pipes and vessels for fast breeder reactors. At present, it is widely used in fossil-fired steam power plants in pressure vessel and piping systems. P91 is tough, weldable and has a creep strength of 94 MPa at 600°C for 100 000 hours [3], [12]. The microstructure of this steel in the as-tempered condition consists of a high dislocation density, which is stabilized by $M_{23}C_6$ and MX carbo-nitrides [13].

In Europe, under the COST program, the pipe steel E911 was developed. This alloy contains 9% Cr and its creep rupture strength is 98 MPa at 600°C for 100 000 hours [12], [14]. NF616 (P92) is a 9% Cr pipe steel, alloyed with C, Mo, W, V, Nb, N, and B that was developed in the second half of 1980s in Japan. Its creep rupture strength is 113 MPa at 600°C for 100 000 hours [12], [14].

3.1.2 Failures

Generally the oxidation resistance improves with increasing Cr content and thus in terms of oxidation, at 650°C, 12% Cr steels are superior to 9% Cr steels [15]–[17]. Within the European COST program, a number of alloys were tested at 650°C for rotor applications. These alloys contained 10-11% Cr and varying amount of V, Nb, N, B, Mo, Mn, Si, and C. The trial steels showed good creep strength for short-term creep tests below 10 000 hours. However in the period between 10 000-20 000 hours, a reduction in creep rupture strength was seen. Based on the results of microstructure characterization of these trial steels, the reduction in creep strength is mainly caused by a phase transformation from small MX to coarse Z-phase particles. The nucleation of Z-phase is a slow process [18], and thus once a Z-phase is formed it starts to consume the neighbouring small MX particles and thus becomes a huge Z-phase, which does not contribute to the creep strength of the material.

Investigation on a number of 9-12 % Cr alloys revealed that in low Cr content alloys (8-9%), even after very long time, very few Z-phase was formed and a fine distribution of MX was preserved. However for a Cr content above 10.5 wt.%, Z-phase precipitation occurred extensively, resulting in a reduction of creep strength [10], [19].

3.2 Physical metallurgy

9-12% Cr steels contain both austenite stabilizing and ferrite stabilizing elements from both interstitial and substitutional elements. The common alloying elements used in 9-12% Cr steels are: Ni, Mn, Co, Si, Mo, Cu, W, Nb, V, Ta, N, B, etc. These alloying elements affect the stability range of austenite and ferrite in the steel.

Austenite stabilizing elements increase the stability range of austenite by dropping A_3 temperature (below A_3 temperature, austenite to ferrite transformation becomes thermodynamically possible) and increasing A_4 temperature (above A_4 temperature, austenite to δ-ferrite transformation becomes thermodynamically possible). Elements like C, N, Mn, Ni, Cu, and Co are austenite stabilizers in iron. On the other hand, the ferrite stabilizer elements such as Si, Mo, W, V, Nb, and Ti decrease the austenite stability region by raising A_3 temperature and dropping A_4 temperature.

By cooling down the steel from the austenite region, phase transformation can occur. This phase transformation can be a diffusion-based transformation (ferrite and pearlite) or a shear process with no diffusion (martensite). Depending on the alloying elements, 9-12% Cr steels consist of martensite or martensite and δ-ferrite. Any increase in the concentration of ferrite stabilizer elements promotes formation of δ-ferrite that is very detrimental to the toughness of these alloys and decreases the creep strength.

Heat treatment of 9-12%Cr steels

Carbon, and many other alloying elements have different solubility in different phases of iron and this is the basis for heat treatment of steel. Heat treatment controls the microstructure through heating and cooling cycles and results in different mechanical properties for different applications. The typical heat treatment for 9-12% Cr steels is an austenitization heat treatment, which is followed by a tempering treatment.

During austenitization, the steel is heated up above the ferrite/austenite transformation temperature. Primary carbides and nitrides are dissolved in the matrix. This is required for later precipitation of fine secondary carbides/nitrides. Austenitization is normally done at temperatures in the range between 1020°C and 1150°C. At a low austenitization temperature, some primary particle might not dissolve during the heat treatment, which results in less solid solution of alloying elements for precipitation of secondary particles. However, some undissolved primary particles are beneficial to restrict the grain growth. During austenitization, these undissolved particles pin the austenite grain boundaries and control the grain growth. At higher austenitization temperature, the concentration of solute elements in the matrix increases. This will result in an increased volume fraction of secondary particles. However, at higher austenitization temperature, there is a possibility to form unwanted δ-ferrite.

When steel is quenched (i.e. cooled rapidly enough that no diffusional transformation occurs during cooling) from austenitic range to room temperature, a brittle and hard phase, martensite, is formed. Martensite is the resulted structure of this diffusionless transformation, shear process, and is a super-saturated solid solution of carbon and possibly nitrogen in iron. Martensite has a body centered tetragonal (bct) structure and the c/a ratio varies with C content. The crystal structure of martensite is relatively closer to the ferrite than the austenite; therefore martensite is generally designated as α′. In martensitic transformation, no diffusion of C occurs and thus the composition of martensite is the same as austenite. The martensitic reaction occurs in steels with specific compositions at a specific temperature range, martensitic start temperature (M_s), and martensitic finish temperature (M_f). The ability of steel to form martensite during cooling or quenching depends on its hardenability. 9-12% Cr steels develop good hardenability and thus even in 12% Cr rotors, martensitic transformation occurs both in the center and at the surface of the forging [20]. The M_s temperature for 9-12% Cr steels is around 400°C and M_f is around 200°C [13]. During quenching, the subgrain structure forms within the prior austenite grains i.e. packet and block boundaries as well as lath boundaries are formed.

Martensite exists in two morphologies, lath martensite and acicular martensite. Acicular martensite is a common morphology in high carbon steels and martensite crystals have the form of thin lenticular plates that are not parallel to each other. Lath martensite is more typical in low and medium carbon steels. Lath martensite are thin plates growing in one direction and parallel to each other. These parallel plates are separated by low angle boundaries. The width of the laths within a packet is in the range of a few microns. The martensite contains a high density of dislocations.

Martensite is a brittle phase and it is essential to apply further heat treatment, tempering, before putting the steel into service. Therefore the tempering treatment is done after austenitization and quenching. During tempering, martensite is heated up below the ferrite/austenite transformation temperature and carbides and nitrides are formed by a diffusion-controlled transformation. The result is a fine distribution of carbides and/or nitrides in a ferritic matrix, which is the basic structure for the family of 9-12% Cr steels.

Tempering in 9-12% Cr steels aims to form secondary precipitates from the super saturated solid solution, reduce internal stresses and recover the dislocation structure. Figure 3.1 shows schematically the microstructure in 9-12% Cr steels after tempering. Some of the dislocations are recovered during tempering. Depending on the

composition of the steel, Laves phase and/or $M_{23}C_6$ particles precipitate on the boundaries and MX precipitates on the boundaries as well as inside grains. Tempering temperature in 9-12% Cr steels is done either in the range of 650°C - 720°C for big components, where high tensile strength is important or in the range of 730°C - 780°C for small components, where toughness is important.

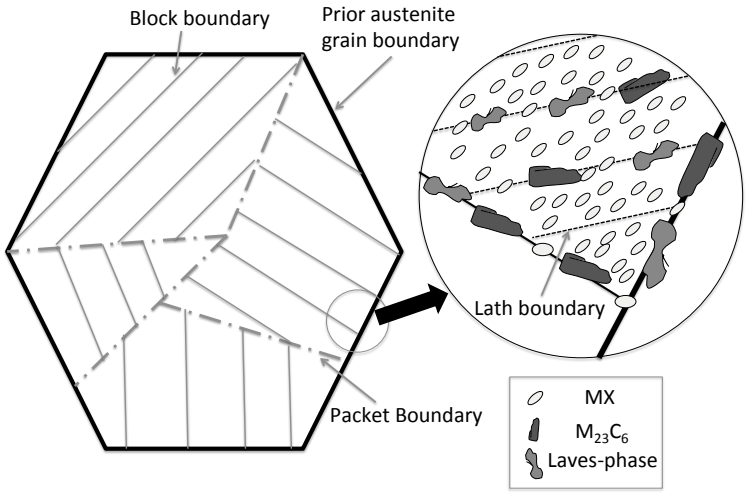

Figure 3.1. Schematic illustration of the microstructure of the tempered martensite in 9-12% Cr steels.

3.3 Precipitates in 9-12%Cr steels

Precipitation processes occur during tempering as well as in service. The precipitation process is typically divided into three stages: nucleation, growth and coarsening.

The nucleation process of precipitates is very important for the creep strength. If a precipitate has a high nucleation rate, a fine distribution of precipitates is obtained, which enhances the mechanical properties. On the other hand if a precipitate has a low nucleation rate, once some precipitates nucleate, they have enough time to consume the necessary elements in their vicinity and thus a low density of precipitates with large sizes are formed, which do not provide optimal precipitation hardening. The nucleation rate is controlled by the availability of the necessary elements in the matrix, thermodynamic driving force, and interfacial energy. Nucleation of precipitates is almost always heterogonous. Non-equilibrium defects such as dislocations, grain boundaries, and inclusions are the possible nucleation sites for precipitates.

When a nucleus has reached a certain critical size, it grows. During the growth process, the sizes of the precipitates increase until the equilibrium volume fraction is reached. The growth rate is controlled by diffusion and the availability of necessary elements in the matrix/particle interface.

Coarsening of precipitates is a result of dissolution of small precipitates and growth of bigger ones while the volume fraction of precipitates remains constant. The coarsening behavior of precipitates is very important for long-term creep strength. Once coarsening process starts, a high number density of small precipitates gradually transforms to a lower number density of big precipitates. The driving force for

coarsening is to decrease the total interfacial energy since a few bigger particles have less surface area compared to many small precipitates. Generally a fine distribution of precipitates gives higher strength. Therefore, coarsening of precipitates results in a loss in strength.

The coherency of the particle with the matrix plays an important role in the coarsening behavior of the precipitate especially if the precipitate and the matrix have different crystal structures; coherent and semicoherent interfaces have a low interfacial energy and therefore coarsen very slowly while incoherent interfaces have a high energy and thus coarsen faster [21].

In tempered martensitic 9-12% Cr steels a wide variety of precipitates may form depending on the composition of the steel and thermal mechanical history. The most important precipitates in this family of alloys are the following:

3.3.1 Metastable precipitates

In 9-12% Cr steels, some metastable precipitates are formed which disappear with time. Some of these precipitates have very short lifespan and dissolve during tempering. M_3C, M_7C_3, and M_2X are typical metastable precipitates in 9-12% Cr steels with short lifetimes. MX is also a metastable precipitates since it will transform to Z-phase but the stability of MX is much higher compared to the other metastable phases and in many steels, MX might stay for the entire lifetime of the component.

M_2X is more stable in steels with a high N content and can still be present for a few thousand hours. They are mainly Cr_2N precipitates with a hexagonal crystal structure and quite large in size and thus undesirable for mechanical properties.

3.3.2 $M_{23}C_6$

$M_{23}C_6$ mainly consists of Cr and C but has minor contents of Fe, Mo, W, and B. $M_{23}C_6$ precipitates are distributed at the prior austenite grain boundary (PAGB), and sub-grain boundaries. They enhance the sub-boundary hardening as well as precipitation hardening, i.e. Orowan stress. In traditional 9-12% Cr steels without B addition, $M_{23}C_6$ precipitates coarsen quickly during creep. Thus it was suggested to limit the C content to 0.02 wt.% to enhance the formation of MX precipitates instead of $M_{23}C_6$. However, recent investigations have shown that the addition of B significantly decreases the rate of Ostwald ripening of $M_{23}(C,B)_6$, and thus the fine distribution of $M_{23}(C,B)_6$ can be maintained in the vicinity of PAGBs during exposure at high temperatures [22]–[24].

3.3.3 Laves phase

The addition of Mo and/or W can result in the precipitation of intermetallic Laves phase with the formula of $Fe_2(Mo,W)$. Laves phase may also contain Cr and certain amounts of Si. Laves phase formation might be detrimental to materials performance mainly due to depletion of W from the matrix and subsequently decreased solid solution strengthening of W. However, the formation of fine Laves phase particles at boundaries enhances the creep strength of the material by retarding the recovery of boundaries [25]–[27]. Thus Laves phase distribution and morphology must be controlled in order to improve the creep strength of the material.

3.3.4 MX

MX precipitates where M represents V, Nb, or Ta and X represents C and/or N, are coherent and semicoherent precipitates, which provide additional strengthening to the 9-12% Cr steels. The coarsening rate of MX precipitates is slow in 9-12% Cr steels and thus they are useful for long-term creep strength [23], [28]. Ti and Al can also produce MX precipitates. The formation of TiN starts already in the liquid state and it is difficult to control the size and distribution of these precipitates. AlN with a hexagonal crystal structure has an incoherent interface and coarsens very quickly [23].

Ta and Nb can react with C and form primary TaC and NbC, which have high temperature stability and are difficult to dissolve during austenitization. These primary particles are normally coarse and do not provide precipitate hardening to the steel [23].

3.3.5 Z-phase

Z-phase is the most stable nitride in 9-12% Cr steels [29] with the empiric formula of CrXN, where X can be Nb, Ta, or V.

The original Z-phase, CrNbN, was first seen in 1950 in Nb alloyed creep-resistant austenitic steels. A fine distribution of rod-like precipitates resulted in precipitating hardening in these alloys. The crystal structure of Z-phase was first characterized in 1972 as tetragonal in austenitic steels [30].

In 1985, Karlsson observed particles with Z-phase composition but with an fcc NaCl crystal structure in austenitic steels after ageing at 750°C. Half of the Nb in these particles were replaced by V and they were thought to be a precursor phase to Z-phase. Danielsen reported that the cubic structure coexists with the tetragonal structure in Z-phase precipitates [31]. Further investigation showed that tetragonal structure is predominant after long-term exposures while cubic structure was found in short-term exposed specimens [32].

In 1986, Schnabel observed a V containing Z-phase in a martensitic 11Cr-1Mo-VNbN steel which showed a dramatic loss in creep and for the first time, Vodarek drew the connection between large Z-phase precipitates and the loss of creep strength. They found that Z-phase grows at the expense of small beneficial MX precipitates. The crystal structure of this V containing Z-phase had smaller lattice parameters compared to the original one and thus Cr(V,Nb)N was named as modified Z-phase [9]. This modified Z-phase precipitates after long-term exposure. Only few coarse particles are formed.

The Cr content has a strong influence on precipitation of Z-phase and the precipitation is much faster in 11-12% Cr steels compared to 9% Cr steels [29], [33].

4. Z-phase strengthened steels

To increase the steam temperature in thermal power plants up to 650°C, it is necessary to use 11-12% Cr steels to ensure a sufficient oxidation resistance. However, it was found that in the 11-12% Cr ferritic martensitic steels that are strengthened by (V,Nb)N particles, precipitation of the thermodynamically stable Z-phase, Cr(V,Nb)N, is unavoidable at long-time service. The Z-phase particles that are formed grow quickly and consume the beneficial MX particles. The coarse Z-phase particles do not contribute to the creep strength of the steel and thus result in premature failures.

The first strategy to tackle Z-phase formation was to delay this phase transformation as much as possible, but it was found that to delay this phase transformation, it is necessary to decrease the Cr content, which will not provide sufficient oxidation resistance for steam temperature of 650°C. Thus this strategy did not work.

Within the European COST 536 ACCEPT action, Danielson and Hald from the Technical University of Denmark proposed a novel alloy design concept, Z-phase strengthening [9]. The idea is to use the Z-phase precipitates as a thermodynamically stable strengthening agent. This means that the composition of the steel and the heat treatments are designed in such a way that a controlled nucleation of finely distributed Z-phase precipitates is achieved after heat treatment or in the early stages of the service (See Figure 4.1). Good creep resistance would be expected, if densely distributed fine Z-phase precipitates can be formed during heat treatment and if they coarsen slowly during service.

Investigations of Z-phase precipitation rate at 600, 650, and 700°C has shown that the Z-phase forms fastest at 650°C [34]; thus the steam temperature of 650°C as well as a high Cr content facilitate the formation of Z-phase.

4.1 Conversion of MX to Z-phase

To achieve a dense distribution of Z-phase, it is necessary to understand the precipitation behaviour of Z-phase. Cipolla has investigated the early stages of Z-phase formation in a model alloy which was designed to form only modified Z-phase based on Cr(V,Nb)N. Cr-rich MN particles were found, which were referred as hybrid particles. The composition profile of hybrid particles showed a smooth transition from a Cr-rich rim to the Cr-poor zone in the centre of the particles. The chemical composition of the rim was close to the composition of Z-phase and the composition of the core was close to the composition of MX. This indicates that Z-phase formation is closely related to MX precipitates and is a result of Cr diffusion from matrix to MX precipitates. For small precipitates less than 100 nm, the whole precipitates transform to Z-phase while for bigger ones, Cr might not diffuse all the way to the core of the precipitates and thus transformation to Z-phase might occur locally [18], [34].

Thus as a result of the Cr uptake from the matrix by MX precipitates, Z-phase is formed. The crystallographic transformation is believed to occur after the chemical transformation. Cubic MX transforms into cubic Z-phase, and it then transforms into tetragonal Z-phase. The cubic Z-phase is believed to be an intermediate structure between cubic MX and tetragonal Z-phase [18], [34].

4.2 Strategy for alloy design

Martensitic 9-12% Cr steels are very complex materials and their alloy development requires optimization of 10-12 alloying elements. The strategy for such an alloy development is based on materials modeling as well as experimental trials. The effects of alloying elements on the microstructure and mechanical properties are discussed below.

A high Cr content of 11-12% is required to accelerate the phase transformation from MX to Z-phase in Z-phase strengthened steels. However, one possible problem with such a high Cr steel is the formation of δ-ferrite. δ-ferrite in these steels reduces strength, ductility and toughness and thus must be considered in alloy development. The Cr equivalent (Cr-eq) value is mostly used as a measure of the possibility for formation of δ-ferrite during solidification of alloy. To avoid δ-ferrite formation, the Cr-eq value must be less than 10. The Cr-eq is calculated by the following equation [35]:

$$\text{Cr-eq} = \text{Cr} + 0.8\text{Si} + 2\text{Mo} + 1\text{W} + 4\text{V} + 2\text{Nb} + 1.7\text{Al} + 60\text{B} + 2\text{Ti} + 1\,\text{Ta} - 20\text{C} - 20\text{N} - 2\text{Ni} - 0.4\text{Mn} - 0.6\text{Co} - 0.6\text{Cu}\ (\text{wt.\%}) \qquad \text{(Equation 4.1)}$$

Nitrogen is well known for increasing the hardenability of steels with low carbon content. Nitrogen contributes to the formation of martensite structure in Z-phase strengthened steels when the C content is limited. Besides, N is a necessary element in formation of Z-phase. Care must be taken in defining the N content. Too high N content may result in the formation of porosities in the cast material.

Too much carbon promotes the formation of $M_{23}C_6$ instead of MX precipitates. Consequently, not only Cr is consumed by $M_{23}C_6$ and less Cr is left in the matrix for Z-phase formation, but also a fine distribution of MX cannot be obtained. Since Z-phase nucleates on MX precipitates, a fine distribution of MX is required. Too high carbon content also results in formation of TaC or NbC, which do not transform to Z-phase.

In Z-phase strengthened steels, a quick phase transformation from fine MX to Z-phase is required. V, Nb and Ta are Z-phase forming elements. The formation of V-based Z-phase is slow [9] compared to Nb-based and Ta-based Z-phase precipitates. Nb-based Z-phase results in coarse precipitates compared to the Ta-based Z-phase [36]. Thus, Ta was selected to achieve a fine distribution of Z-phase.

Tungsten is added to provide further solid solution hardening and precipitate hardening by forming Fe_2W Laves phase. However, too high content of W might result in formation of δ-ferrite and reduction of toughness. Mn, Ni, Co and/or Cu are added to the steel to suppress the formation of δ-ferrite. Too high content of these alloying elements reduces the ability to temper the alloy at high enough temperatures. Co is believed to enhance the Z-phase formation [9]. Si is added to the steel to improve the oxidation resistance and steelmaking process.

Boron is added to the steel to improve the hardenability. It also contributes to the creep strength of the alloy by grain boundary strengthening. B addition to the steel decreases the rate of Ostwald ripening of $M_{23}C_6$ and thus enhances the precipitation

hardening [24]. The B and N contents must be carefully designed during alloy development since it might result in formation of massive BN particles during normalizing at high temperatures. Therefore, less N is left in the matrix for precipitation of Z-phase [3].

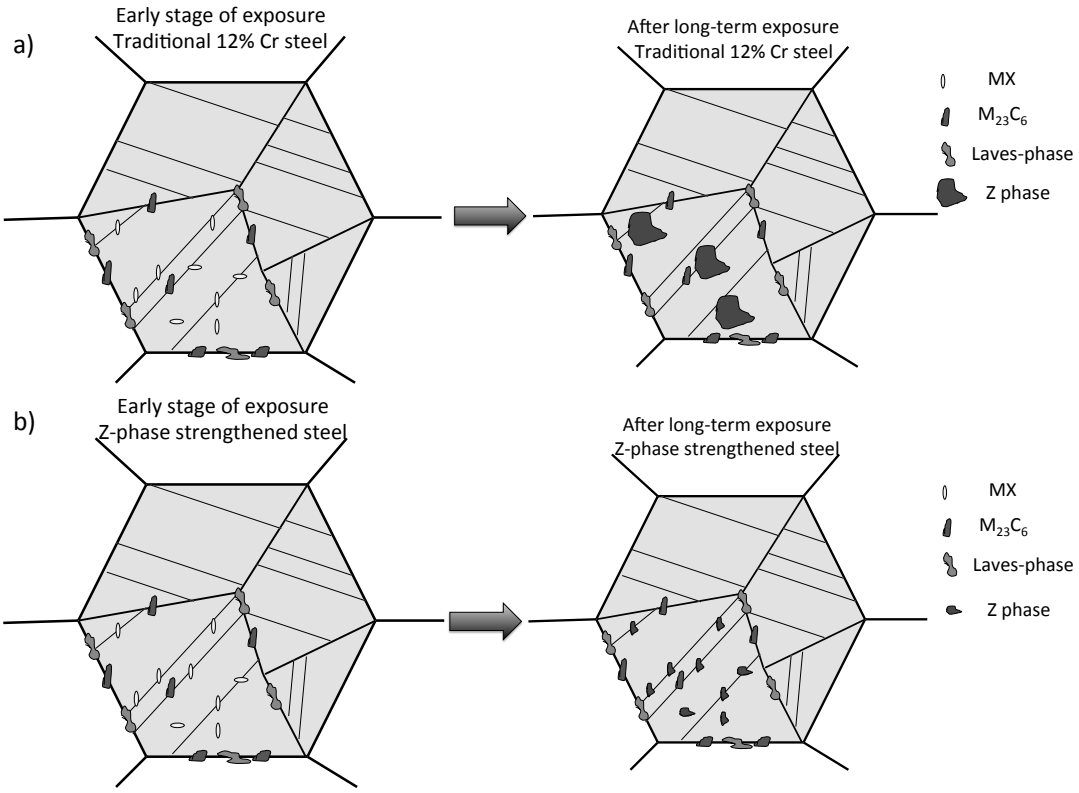

Figure 4.1. Schematic illustration of a) traditional 12% Cr steels b) Z-phase strengthened steels.

5. Experimental methods

The experimental investigation in this thesis was mainly aimed at understanding the precipitation reactions and phase transformations during heat treatment and ageing. Several trial steels in the as-tempered condition and aged for different times were characterized carefully. To obtain reliable results on the chemistry of the precipitates, their morphology and crystal structure, a number of techniques and sample preparation methods were employed. Scanning electron microscopy (SEM) was mainly used to obtain an overview of the microstructure of 9-12% Cr steels in the as-tempered condition; transmission electron microscopy (TEM) was mainly used to study the precipitates and their crystal structure, and atom probe tomography (APT) was the main technique used to determine the chemistry of precipitates as well as the matrix.

5.1 Studied materials

In this thesis, two Z-phase strengthened martensitic 12% chromium steels were studied. The chemical compositions of these two alloys are presented in Table 5.1.

Table 5.1. Chemical composition of investigated 12% Cr steels (Fe in balance).

Steel		Ni	Co	Cr	W	Ta	C	B	N	Si	Mn	Cu
12Cr7CoTa	at%	0.48	7.01	12.84	0.89	0.12	0.02	0.02	0.13	0.60	0.49	0
-uLC	wt%	0.50	7.30	11.79	2.90	0.39	0.005	0.004	0.033	0.30	0.48	0
12Cr3CoTa	at%	0.18	3.35	13.13	0.76	0.11	0.28	0.03	0.20	0.62	0.22	1.73
-HC	wt%	0.19	3.50	12.10	2.47	0.36	0.06	0.006	0.049	0.31	0.21	1.95

The alloy design concept for 12Cr7CoTa-uLC (ultra-Low Carbon) model steel was based on using a fine distribution of Z-phase as strengthening agent instead of MN particles in traditional 9-12% Cr steels. Low C content in this trial steel suppresses the formation of carbides and this provided the possibility to study the strengthening effect of Z-phase without interferences from carbides. The high Cr content, 12%, ensures the good corrosion resistance of this alloy. Besides, this high Cr content is a necessary prerequisite to accelerate the formation of Z-phase precipitates. Formation of a dense distribution of Z-phase during heat treatment together with slow coarsening rate during service provides good creep resistance. A high amount of Co was required to balance between austenite stabilizers and ferrite stabilizers. It is also believed that a high Co content accelerates the Z-phase formation. This high amount of Co makes this alloy slightly expensive for industrial applications. Besides, the produced alloy showed weak toughness properties. Thus, the second alloy was produced aiming at a more industrially acceptable chemical composition and improved toughness properties. The second trial steel, 12Cr3CoTa-HC, contains more C and less Co and an addition of Cu compared to 12Cr7CoTa-uLC.

Both trial steels were produced in 80 kg ingots by vacuum induction melting. The ingots were hot rolled into 20 mm thick plates. Both steels were austenitized at 1150°C and quenched by air-cooling to room temperature.

For the 12Cr7CoTa-uLC trial steel, aging and creep tests were carried out on samples tempered either at 650°C for 24 hours or 720°C for 6 hours. Creep tests were performed under a constant load of 120, 100 and 80 MPa, using specimens of 8 mm in gauge diameter and 50 mm in gauge length. Samples aged for 24, 1005, and 10,000 hours were used for microstructural investigation.

The 12Cr3CoTa-HC steel underwent double step tempering of 6 hours at 650°C followed by 6 hours at 740°C. During the first step of tempering, Cu precipitates out and thus the amount of austenite stabilizer elements decreases and thus the A_1 temperature increases allowing a higher tempering temperature of 740°C in the second step. The 12Cr3CoTa-HC steel was studied in the as-tempered condition and after 1000 hours ageing at 650°C.

5.2 Scanning electron microscopy

SEM was mainly used to obtain an overview of the microstructure and image the grain structure, lath boundaries, and particles larger than 10 nm. The following short description of SEM is based on the book by J.Goldstein et al. [37]. The two major parts of an SEM are the electron column and the control console. In the electron column, electrons are emitted from an electron gun, nowadays often a field-emission gun, with an energy adjustable in the range of 0.1-30 keV. Electromagnetic lenses control the path of electrons in the column with a pressure of roughly one billionth of atmospheric pressure. The control console contains a viewing screen, knobs and computers that control the beam.

The electrons emitted from the electron gun are accelerated to a high energy. They travel through electromagnetic lenses and form a focused electron beam on the specimen. Electrons interact with the specimen and different signals are generated from the so-called electron-material interaction volume. The size of interaction volume plays an important role in interpreting the results obtained from SEM. Different parameters such as the accelerating voltage, the atomic number of elements in the specimen and density of the specimen affect the interaction volume size. Scanning coils in the column deflect the beam in X and Y direction over a rectangular area on the specimen surface. The generated signals from the interaction volume are then recorded by different detectors for each beam position and form a two-dimensional image of the specimen.

Secondary and backscattered electrons and characteristic X-rays are the major signals produced within the interaction volume. Secondary electron (SEs) are used to obtain topographical images of the specimen since the possibility of emitting SEs from the edges is higher compared to the flat areas on the specimen surface. SEs are produced by inelastic scattering of the incident beam and have low energies. Backscattered electrons (BSEs) are produced by elastic scattering of the incident electrons within the interaction volume. BSEs have energies close to the energy of the incident electrons. BSEs carry information on the composition of the specimen. By considering the fact that the probability of elastic scattering increases by increasing the atomic number, Z, it is possible to obtain images with compositional contrast of the specimen. Areas containing heavier elements produce more BSEs, resulting in higher intensities compared to the areas containing light elements in the image. The third important signals produced within the interaction volume are characteristic X-rays, which are

discussed in more detail in section 5.4. Figure 5.1 summarizes different signals and detectors in a SEM.

In this thesis, BSEs and X-rays are often used for characterization of different particles. Laves phase contains W which is a heavy element and thus it gives a very bright contrast compared to $M_{23}C_6$ and Cu particles by using BSE imaging. MX and Z-phase particles also contain a heavy element, Ta, and thus BSEs are often used to show the distribution of these particles within the steel matrix. The difference between the contrast of Z-phase and Laves-phase in BSE imaging is so small that one needs to employ EDXS to distinguish between these particles.

The SEM results presented in this thesis were obtained using a Zeiss Ultra 55^{TM} SEM operated at accelerating voltages ranging from 2-15 kV. The energy and angle Selective Backscattered (EsB) detector in the SEM provids the possibility to obtain high-resolution backscattered electron images that can clearly reveal precipitates of nanometre size. When the SEM is operated at a rather low accelerating voltage, the low energy loss electrons that carry chemical information from the very surface (a few nanometres) of the material can be collected by this EsB detector installed inside the electron column. This gives a SEM micrograph with chemical information and a resolution as high as 10-20 nm, which is much better compared to the resolution of traditional BSE detectors, 0.5 micron.

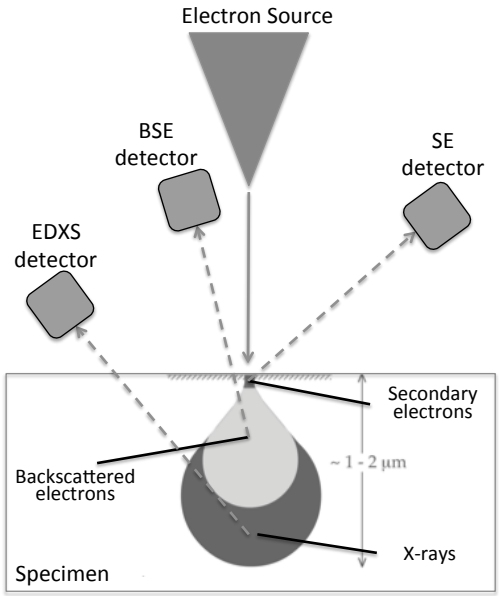

Figure 5.1. Schematic drawing showing the electron source, different signals and frequently used detectors in an SEM.

5.3 Transmission electron microscopy

A TEM consists of an electron gun, electromagnetic lenses, and a viewing screen that are all enclosed in a vacuum system. The accelerating voltage in a TEM, 100-300 kV, is much higher compared to that in a SEM, maximum 30 kV. The specimen has to be electron transparent meaning that the electrons emitted from the gun have to pass through the specimen. Thus in a TEM, the transmitted electrons from an ultra thin

specimen (thickness <100nm) are detected and used for imaging [38]. Figure 5.2 schematically shows a TEM.

The incoming electron beam interacts with the specimen and results in elastically (no loss of energy) and inelastically (losing their energy) scattered electron, and X-rays. The obtained contrast in the TEM mode and the intensity distribution in diffraction patterns mainly result from elastically scattered electrons. Electron diffraction is a powerful technique that was used to identify the crystal structure and lattice parameter of phases. Inelastically scattered electrons mostly provide information on the chemistry of the specimen. Energy-loss electrons and X-rays are often used to collect information on the chemistry of the material.

In the bright field (BF) mode of TEM, the objective aperture is inserted in the back focal plane of the objective lens, and only the direct beam passes through the aperture. The acquired image is a result of weakening the transmitted beam by its interaction with the specimen. Mass-thickness and diffraction contribute to the contrast of image. Areas containing heavy elements and thick areas appear with a dark contrast. Areas with different crystal structure provide different contrast in the image (see Figure 5.3 a).

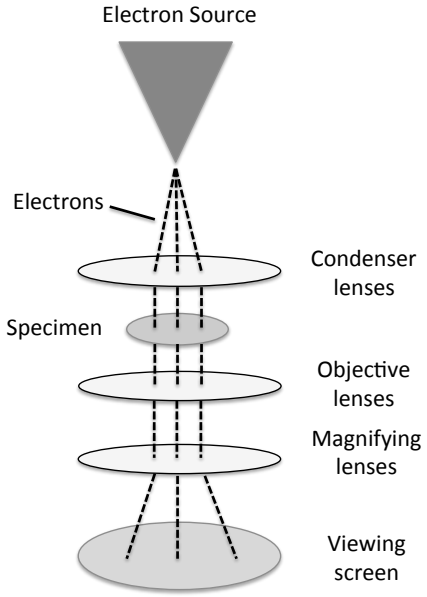

Figure 5.2. Schematic drawing showing the electron source, electromagnetic lenses, specimen, and viewing screen in TEM.

In the STEM mode, the electron optics is similar to that in a SEM. The electron beam is focused on the plane of the specimen and scans over the specimen. In the STEM mode compared to SEM, instead of SEs and BSEs, the transmitted electrons through the electron transparent specimen are used to form images. A so-called High-Angle Annular Dark-Field (HAADF) detector provides an image with Z-contrast (Z: atomic number). The areas with greater Z and/or thickness scatter electrons more strongly and thus they appear brighter using HAADF, see Figure 5.3 b.

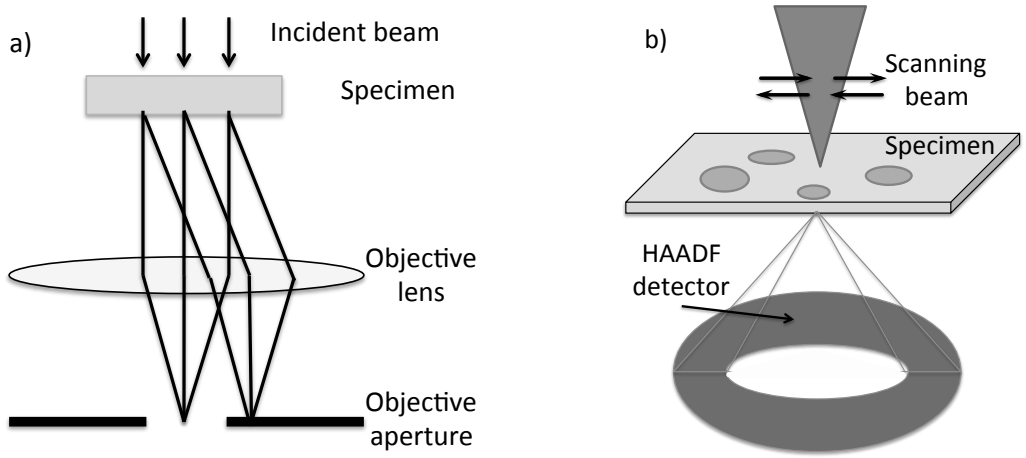

Figure 5.3. Schematic drawing showing a) the bright field imaging mode in TEM b) the STEM mode.

There are generally two ways to produce diffraction pattern in the TEM; using the selected area aperture to form selected area diffraction pattern (SADP) or by using a convergent beam to form convergent beam electron diffraction (CBED). Since the smallest SAD aperture (100 nm) was bigger than the size of precipitates (around 50 nm), to avoid any contribution from the matrix to the diffraction pattern of the precipitates, CBED was mainly employed to characterize the precipitates.

In this thesis, imaging was done in both TEM and STEM modes. Moreover, EDXS and diffraction patterns of precipitates were collected to identify their type and crystal structure. Two TEMs were employed, a FEI Tecnai T20 TEM equipped with a LaB_6 gun operated at 200 kV, and a FEI Titan 80-300^{TM} (S)TEM, equipped with a Schottky field emission gun, operated at 300 kV.

5.4 Energy dispersive X-ray spectroscopy

The incoming electrons interact with the specimen in both SEM and TEM and create characteristic X-rays radiation by ionizing atoms in the specimen. An electron from a higher energy state in an ionized atom travels to a lower energy state and the energy difference can result in X-ray radiation. Since the difference in energy between two electron shells is unique for each atom, X-rays of *characteristic* energies are used for analysis. The emitted X-rays are collected using a detector mounted above the specimen. Analyzing the intensity distribution of X-rays as a function of energy tells you which elements are present in the material and their concentration. The obtained information from Energy Dispersive X-ray Spectroscopy (EDXS) can be treated both quantitatively and qualitatively. The simplest way to acquire EDXS is to position the electron beam on the feature of interest and acquire a spectrum (spot analysis). It is also possible to collect the EDXS spectra while scanning the electron beam over the specimen (EDXS mapping), which provides elemental mapping of the material.

5.5 Atom probe tomography

APT is by far the most powerful analytical method to study the chemical composition at an atomic level. It determines the chemical composition based on counting the number of atoms of each type. APT is the first instrument capable of determining the

species of a single atom from the surface of a needle-shape specimen. A needle-shaped specimen with a tip radius of less than 50 nm is subjected to a very strong positive DC potential in an ultra-high vacuum chamber (≈10^{-9} Pa) at cryogenic temperatures (20-100 K). An additional voltage or laser pulse is superimposed on the specimen and results in a controlled ionization of surface atoms of the needle; this process is called field evaporation. This method is destructive in nature and the ionized atoms leave the surface of the specimen and are accelerated towards a position sensitive detector through a circular aperture that is held at zero potential and serves as a counter electrode, see Figure 5.4. The position sensitive detector registers the coordinates (X and Y) of the atomic or molecular ion. The time of flight starting from the superimposed pulse until the ion reaches the detector is measured and by considering that only the surface atoms are ionized, gives the possibility to evaluate the spatial position and atomic mass for each ion. Thus a 3-dimentional reconstruction of the tip can be created.

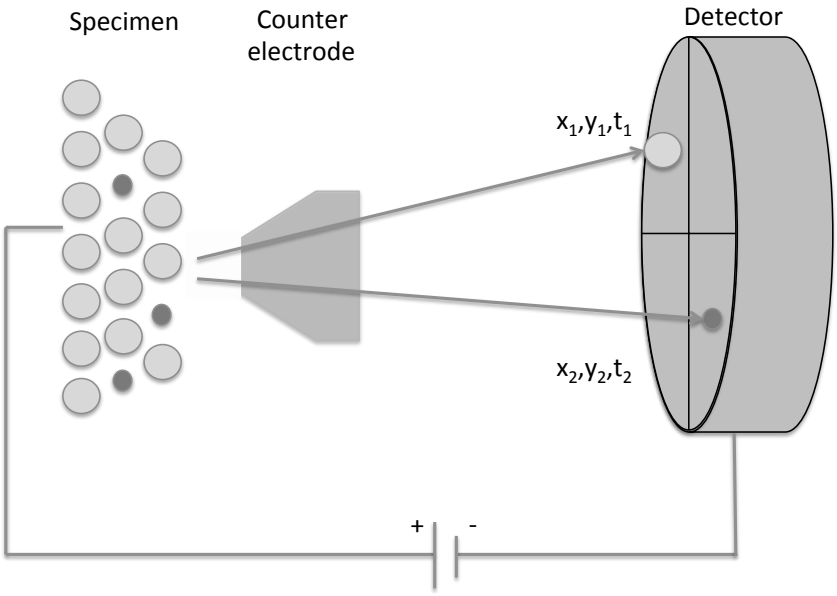

Figure 5.4. Schematic drawing of experimental setup in the APT.

An APT measurement of a suitable specimen can contain tens of millions of atoms in a volume of 100×100×500 nm^3. Each event on the detector is registered via two coordinates as well as a mass-to-charge ratio and processing this huge amount of data requires a proper computing power.

An Imago LEAP 3000X HR local electrode APT was employed to study the chemical composition of precipitates. During analysis the specimen was held at a temperature of 55-56 K. The instrument was operated in pulsed laser mode with a laser pulse energy of 0.3 nJ. The data collected by the instrument was further analyzed using the IVAS 3.4.6 software.

5.6 Specimen preparation

Several specimen preparation methods can be employed for microstructure investigation of steels. Each method might introduce some artefacts and it is very

important to identify these artefacts for a proper understanding of the microstructure. We have employed three different methods of sample preparation: mechanical polishing, electropolishing, and ion milling.

Specimen preparation for electron microscopy

Mechanical grinding and polishing is the most common method that was employed to prepare specimens. This relatively easy and quick method provided specimens good enough for a SEM investigation. However, the surface of the specimen often contained scratches induced by this preparation technique.

For electropolishing, the specimen needed to undergo first mechanical polishing and then chemical polishing. An electrolyte of 10% perchloric acid in methanol was used at -30°C to electropolish disks (3 mm diameter and 100-200 μm thick) using a Struers Tenupol Twin Jet electropolisher until perforation. The area adjacent to the hole, very thin (<100 nm), was used for TEM investigations. By considering the fact that electropolishing provides damage free and smooth surfaces, the electropolished specimens were also used for SEM investigations. However, with this method, Cu particles were dissolved in the electrolyte during electropolishing and holes were left in the matrix.

Ion milling and polishing is the most time-consuming method compared with aforementioned techniques. A Fischione low angle ion milling and polishing system was employed to prepare TEM specimens with large electron transparent areas. In this technique, emitted argon ions from ion sources are used for milling the 3 mm diameter disks. Compared to electropolishing, preparing specimens by ion milling has the advantage of leaving Cu particles intact for TEM analysis. This method also provides better specimens for SEM analysis using BSE detector. However, SE micrographs show a wavy surface as a result of prolonged ion milling.

Specimen preparation for APT

To produce a needle-shaped specimen from metallic rods, electropolishing was employed. First a low speed saw was used to cut slices of 0.3 mm from a bulk specimen. Then rods of the size $0.3\times0.3\times15$ mm^3 were cut using the same saw. Rods were mounted in small 0.5 mm diameter aluminum holders. Then electropolishing was done in two steps as shown in Figure 5.5. In the first step, a thin layer of electrolyte containing 10 vol.% perchloric acid in 2-butoxyethanol floats over trichloroethylene (inert liquid). Then by applying a voltage, a neck was created in the part of the material that was immersed in the electrolyte. In the second step, the whole specimen was placed in a weaker electrolyte, 2 vol.% perchloric acid in 2-butoxyethanol, and slow polishing continued until the lower part of the specimen dropped and two sharp needles were created.

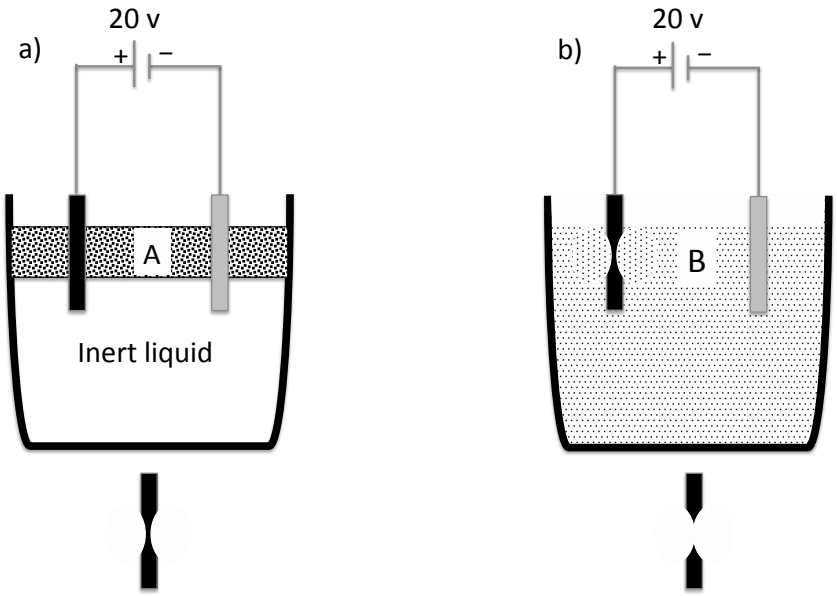

Figure 5.5. Schematic showing two-step electropolishing to produce APT specimens. a) stage 1 to produce a neck in the specimen, electrolyte A is 10 vol.% perchloric acid in 2-butoxyethanol b) stage 2 to obtain a sharp needle, electrolyte B is 2 vol.% perchloric acid in 2-butoxyethanol.

6. Summary of results and discussion

In this chapter, a summary of obtained results is given and discussed. Moreover, some unpublished data from ongoing research are provided. The results are presented based on the trial steels.

6.1 12Cr7CoTa-uLC trial steel

The trial steel 12Cr7CoTa-uLC (ultra Low Carbon) was especially designed in order to study the effect of Z-phase strengthening and if a fast transformation from MX to Z-phase precipitates is feasible while maintaining a fine distribution of Z-phase. The calculated Cr-eq based on equation 4.1 was approximately 9.2, which is less than 10 and as expected no δ-ferrite was formed in the trial steel. The PAG size in this trial steel was determined to be 114 μm.

Due to the very low C content in this trial steel, no $M_{23}C_6$ carbides were present and this enabled the study of the strengthening effect of Z-phase without interference from carbides. The high Cr content of 11.7 wt.% accelerated the Z-phase formation compared to the 9% Cr steels. Relatively large amount of Co, 7.3 wt.%, was added to the steel to enhance the phase transformation from MX to Z-phase as well as suppressing δ-ferrite formation.

The 12Cr7CoTa-uLC trial steel showed a typical martensitic structure. In this trial steel mainly two family of precipitates exist, Laves phase and Z-phase. In Figure 6.1 a), a HADDF/STEM micrograph of the trial steel aged for 24 hours at 650°C is shown, where PAGB, lath boundaries, and Laves phase precipitates are highlighted.

The composition of the matrix was accurately investigated using APT in the specimen aged for 24 hours and the contents of Ta, N, C, and B were almost zero indicating that the whole volume fraction of Z-phase has precipitated. The blade-like precipitates formed after 24 hours of ageing at 650°C were identified as Z-phase based on their composition. This trial steel had a poor impact toughness, which is believed to be the result of continuous Laves phase formation along the PAGBs.

The aged specimen for 1005 hours at 650°C was investigated using EDXS and electron diffraction in TEM. These studies showed that small precipitates rich in Ta and Cr, ≈50 nm, are Z-phase particles with tetragonal crystal structure. Figures 6.1 b, c, and d show a STEM/HAADF micrograph obtained from the trial steel after 1005 hours ageing at 650°C together with typical EDXS measurements from Laves phase and Z-phase. After 10 000 hours ageing, Z-phase precipitates were densely distributed in the matrix with the size smaller than 100 nm, which suggests a slow coarsening rate for Z-phase precipitates.

The effect of B on retarding the coarsening of $M_{23}C_6$ is well known. The existence of B at the interface of Z-phase precipitates and matrix was shown using APT. The B at the interface is believed to be beneficial, since it may decrease the interfacial energy of the precipitates, and thus retard their coarsening rate.

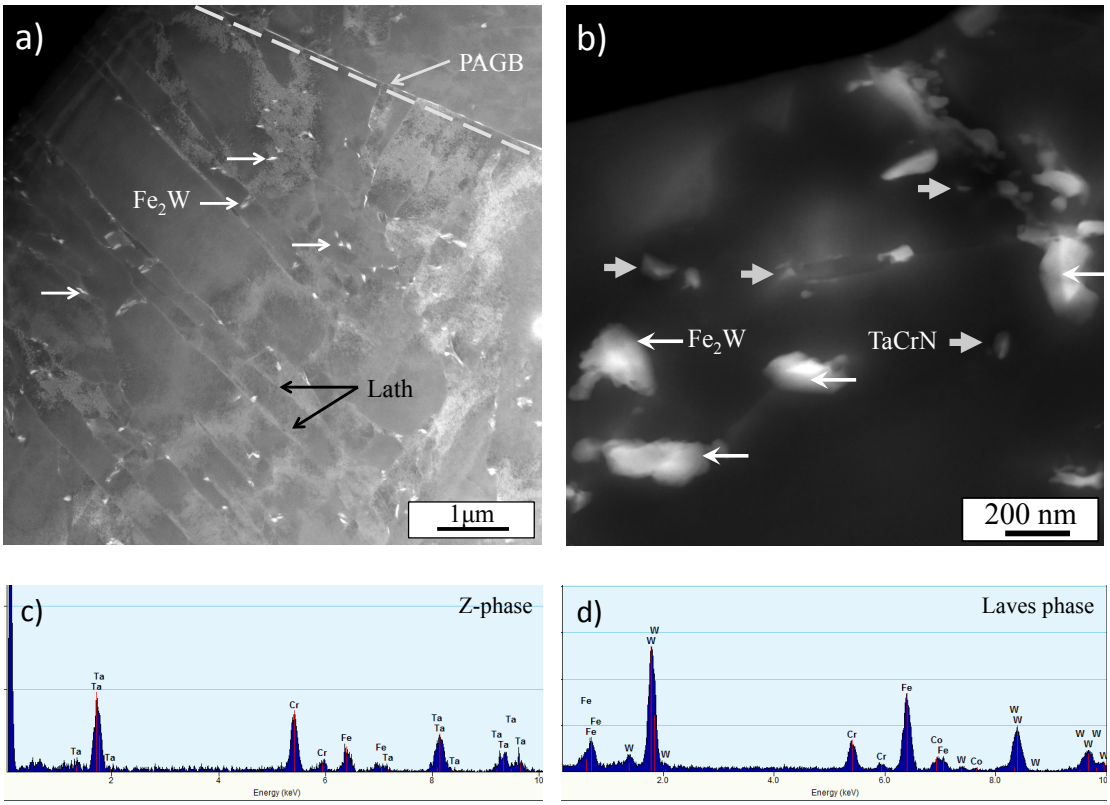

Figure 6.1. STEM/HAADF micrographs of 12Cr7CoTa-uLC trial steel a) aged for 24 hours and b) aged for 1005 hours at 650°C. Typical EDXS obtained from c) Z-phase and d) Laves phase.

6.2 12Cr3CoTa-HC trial steel

Compared to the 12Cr7CoTa-uLC trial steel, 12Cr3CoTa-HC trial steel contains Cu, relatively more C and less Co. The Cr-eq value for this trial steel is approximately 9.6 and as expected no δ -ferrite was formed. The PAG size was determined to be 50 µm. The effects of the changes in the alloying element contents were studied in detail in the as-tempered condition and after ageing at 650°C.

The effect of C addition:

Carbon plays an important role in the precipitation behavior of steels. The C addition in the 12Cr3CoTa-HC trial steel provided more precipitation strengthening by forming $M_{23}C_6$ compared to 12Cr7CoTa-uLC. However, it affected the phase transformation from MX to Z-phase. Formation of secondary precipitates of type Ta(C,N) and their existence even after 1000 hours ageing at 650°C suggests that the phase transformation from Ta-carbonitrides to Z-phase is slower than from Ta-nitrides. Figure 6.2 shows the APT results obtained from 12Cr3CoTa-HC in the as-tempered condition. As can be seen, the precipitation process in 12Cr3CoTa-HC trial steel is much more complicated; Ta(C,N), Z-phase and Cr-rich precipitates coexist. The Cr-rich precipitates are believed to be a metastable phase and disappear after short-term ageing. However the co-existence of Z-phase and Ta(C,N) might be negative for long-term creep tests.

Lower Co content in 12Cr3CoTa-HC trial steel might be another reason for slower transformation from Ta(C,N) to Z-phase, since it is believed that Co accelerates the Z-phase formation.

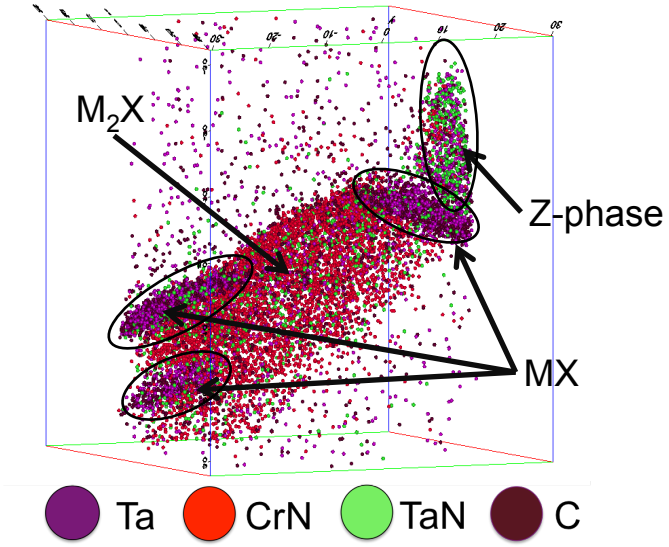

Figure 6.2. Reconstruction of an APT data set showing precipitates in 12Cr3CoTa-HC trial steel in the as-tempered condition. Box size 60*60*60 nm.

The effect of Cu addition

The Cu was added to the 12Cr3CoTa-HC trial steel for different purposes. Cu is an austenite stabilizer and suppresses the δ-ferrite formation. However, it decreases the A_1 temperature and thus tempering at higher temperatures is not possible. To solve this issue, a double step tempering was designed, the first step was tempering at low temperature of 650°C and second step at 740°C. Cu precipitates during the first step of tempering as Cu particles and therefore the A_1 temperature rises allowing us to do the second step of tempering at higher temperature of 740°C.

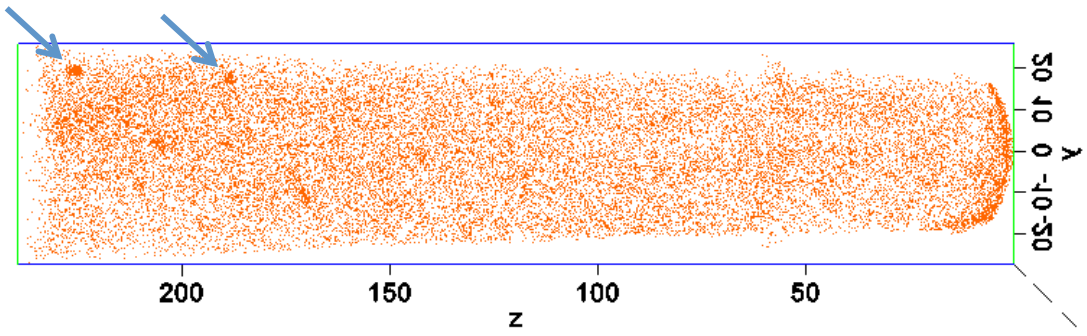

Figure 6.3. Reconstruction of an APT dataset showing the distribution of Cu ions in the12Cr3CoTa-HC trial steel in the as-tempered condition. Some nano Cu particles are seen.

Cu particles formed during the first step of tempering act as nucleation sites for Laves phase and thus the formation of continues Laves phase at PAGBs is avoided.

Formation of $M_{23}C_6$ can also affect the morphology of Laves phase; formation of $M_{23}C_6$ results in local depletion in Cr and relatively high local concentration of W in this region, which precipitates as Laves phase. The improved morphology of Laves phase is believed to be the reason for improved toughness in 12Cr3CoTa-HC compared to 12Cr7CoTa-uLC. The Cu particles in the as-tempered condition are shown in Figure 6.3.

Figure 6.4 shows SEM backscattered electron micrographs of 12Cr3CoTa-HC trial steel aged at 650°C for 5500 hours at different magnifications. Particles with gray contrast are mainly $M_{23}C_6$, Cu or in some rare cases Cr_2N. Laves phase particles have bright contrast with a size in the range of 100-500 nm. Ta(C,N) and/or Z-phase also exhibit bright contrast but they are much smaller, approximately 100 nm.

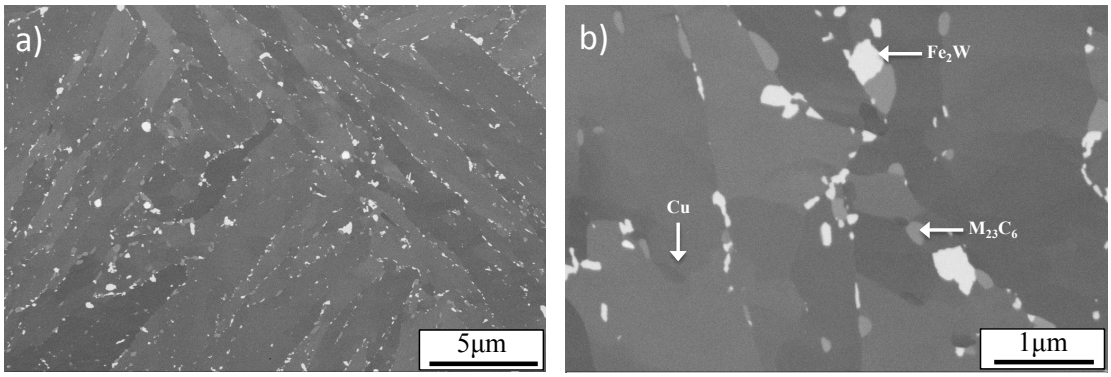

Figure 6.4. SEM/BSE micrograph of 12Cr3CoTa_HC after ageing at 650°C for 5500 hours at different magnification.

6.3 11Cr3Co series of trial steels (Unpublished)

Based on the microstructure investigations and creep results, 3 other trial steels were designed and produced. The compositions of new trial steels are provided in Table 6.1. The following issues were considered for designing these new trial steels:

- The C content was selected between 12Cr7CoTa-uLC and 12Cr3CoTa-HC to get faster transformation from Ta(C,N) to Z-phase.
- The Cr content was slightly lower compared to the first and the second generation of trial steels in order to get higher A_1 temperature and therefore temper at higher temperatures.
- The B and N contents were designed in order to minimize the formation of BN particles.
- The effect of combining Ta and Nb on the Z-phase formation was investigated.

Table 6.1. Chemical composition of 11% Cr trial steels (Fe in balance).

Steel		Cr	Co	Si	W	Mo	Cu	Mn	Ni	C	N	Ta	Nb	B
11Cr3CoTa -LC	at.%	12.1	2.7	0.68	0.61	-	1.8	0.12	0.17	0.13	0.18	0.11	-	0.02
	wt.%	11.2	2.8	0.34	2.0	-	2.0	0.12	0.18	0.03	0.045	0.35	-	0.004
11Cr3CoTaNb -LC	at.%	12.1	3.1	0.64	0.64	-	1.9	0.13	0.16	0.14	0.17	0.06	0.10	0.03
	wt.%	11.2	3.2	0.32	2.1	-	2.1	0.13	0.17	0.03	0.042	0.19	0.16	0.005
11Cr3CoTa -MC	at.%	12.2	3.0	0.47	0.56	0.3	-	0.12	0.20	0.24	0.15	0.14	-	0.02
	wt.%	11.1	3.1	0.23	1.8	0.5	-	0.12	0.21	0.05	0.036	0.43	-	0.004

In the 11Cr3Co series of trial steels, we aim to find the optimal C/N ratio to achieve a quick transformation from MX to Z-phase. To do this, two trial steels were designed based on a low carbon content, (LC), and one trial steel with a medium carbon content, (MC). So far Z-phase precipitates based on Nb, Nb-V, and Ta have been studied. The behavior of Z-phase based on Ta-Nb combination is still unknown. Thus 11Cr3CoTaNb-LC was designed to study the Cr(Ta,Nb)N Z-phase and its precipitation and coarsening rate.

The trial steels were austenitized at 1100°C for 1 hour, and then underwent double step tempering of 4 hours at 650°C and 2 hours at 750°C. The trial steels were investigated in the as-tempered condition and after ageing for 1 month at 650°C.

In 11Cr3Co series of trial steels, the B and N contents were designed in order to suppress the formation of detrimental BN particles. The results obtained from quantitative SEM measurements are summarized in Figure 6.5. As can be seen, the BN volume fraction in 11Cr3Co family of trial steels is less than that in the 12Cr3CoTa-HC one. The mean size of BN particles in all trial steels was approximately 1 μm.

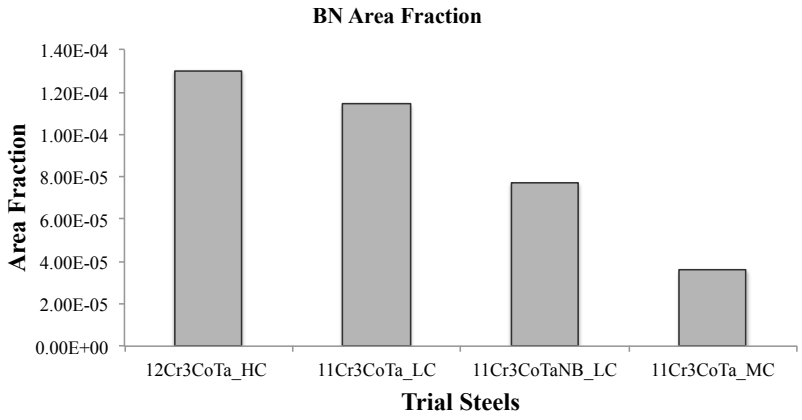

Figure 6.5. BN area fraction in the trial steels.

Quantitative SEM investigation on the size distribution of MX precipitates in the trial steels are summarized in Figure 6.6. However, 11Cr3CoTa-LC (Low Carbon) trial steel has the finest size distribution of MX particles. The peak value for the size distribution of 11Cr3CoTa-LC is expected to be for precipitates with sizes less than 80 nm.

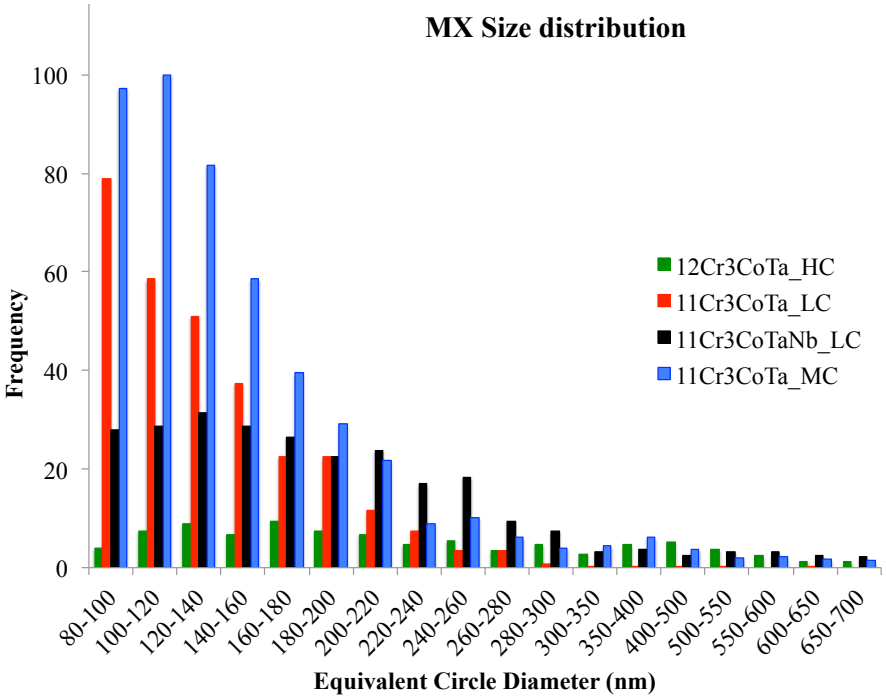

Figure 6.6. The size distribution of MX particles in the trial steels.

APT was employed to measure the chemical composition of the small precipitates in 11Cr3CoTa-LC trial steel. Figure 6.7 shows the distribution of Cu, C, Ta and TaN ions in one of the 11Cr3CoTa-LC trial steel specimens in the as-tempered condition. Some Cu particles less than 10 nm in size were formed in the trial steel. Besides, three Ta(C,N) precipitates can be seen in the C, and Ta + TaN ion maps. These precipitates

contain approximately 40 at.% Ta, 30 at.% C, 15 at.% N, and 8 at.% Cr. The Cr diffusion to the MX precipitates has started. However, the Cr concentration is still too low and the carbon concentration is too high.

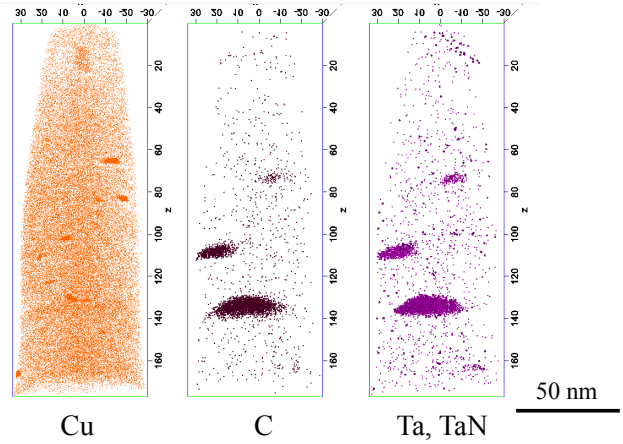

Figure 6.7. Reconstruction of an APT dataset showing the precipitates in 11Cr3CoTa-LC trail steel in the as-tempered condition.

The preliminary results obtained from TEM shows that the Ta-rich precipitates in 11Cr3CoTa-LC trial steel preserve their small size after 1 month of ageing at 650°C, see Figure 6.8. The EDXS results show that the small precipitates are rich in Ta and Cr. According to the APT measurement, the MX precipitates contain approximately 38 at.% Ta, 20 at.% C, 20 at.% N, and 16 at.% Cr i.e. more N and Cr and less C compared to the MX in the as-tempered condition. These results indicate that the phase transformation from MX to Z-phase is occurring but it is not completed yet.

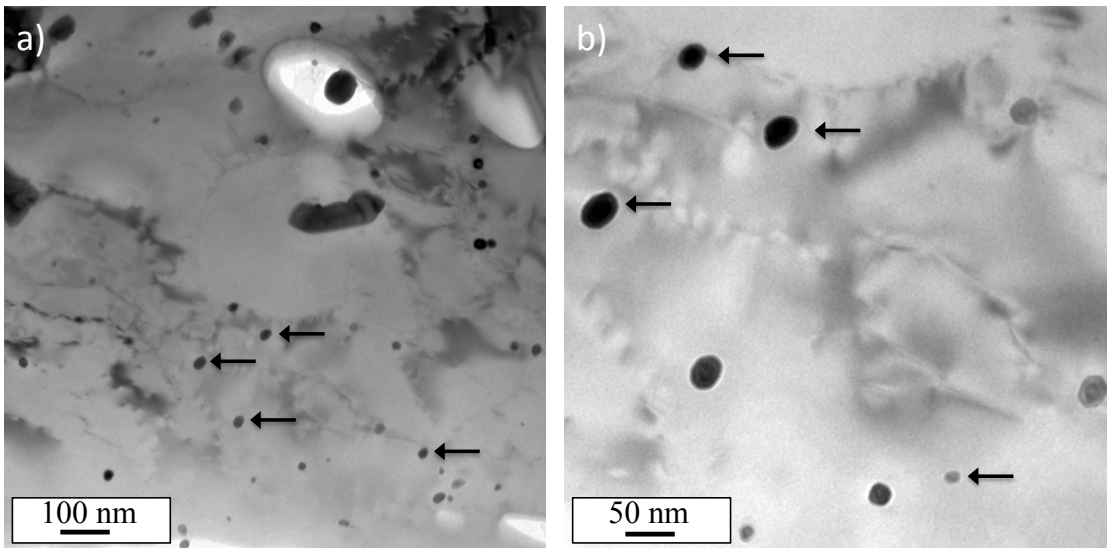

Figure 6.8. TEM bright field micrograph showing small MX precipitates in the 11Cr3CoTa_LC trial steel aged for 1 month at 650°C.

7. Summary and outlook

One aim of this study was to investigate the feasibility of using Z-phase as a strengthening agent in 12% Cr steels. To achieve Z-phase strengthened steels, a quick precipitation of a finely distributed Z-phase is required. With the first trial steel, 12Cr7CoTa-uLC, it has been shown that by using high Cr and Co content combined with an ultra low carbon content it is possible to achieve a fine distribution of Z-phase precipitates. However, this alloy has poor toughness. Besides, an ultra low C content, as well as a high Co content, makes this alloy not so feasible from a mass production point of view.

The second trial steel, 12Cr3CoTa-HC showed improved toughness. However, the quick transformation from MX to Z-phase was not achieved, due to the high C content. Thus, a new series of trial steels were designed to explore the optimum C content to achieve a fast transformation from MX to Z-phase along with optimum toughness. Investigation of Z-phase precipitation in the recently designed alloys, 11Cr3Co series of trial steels, is our next step to find the optimum C content in Z-phase strengthened steels.

Besides Ta, Nb and V are also Z-phase forming elements. CrNbN and Cr(V,Nb)N Z-phase precipitates have been studied by a number of researchers. However, the behavior of Cr(Ta,Nb)N Z-phase has not been investigated. We plan to study the effect of combing Ta and Nb on the Z-phase formation and coarsening.

An applied stress appears to accelerate the coarsening rate of $M_{23}C_6$ precipitates [26]. A similar effect may also occur in Z-phase precipitates. So far we have studied the aged specimens that were not subjected to any stress. The effect of creep deformation on Z-phase precipitation and its coarsening rate will be investigated.

M_6X is another stable phase in 9-12% Cr steels that forms as big particles and is detrimental for creep properties. By considering the high Cr and N content in our Z-phase strengthened steels, the formation of this phase will be studied in more detail.

8. Acknowledgments

Since I have started my PhD studies, I have gotten to know many wonderful people whose support has made my journey even more enjoyable. I would like to express my gratitude to all of them.

My sincere appreciations go to my supervisors Assistant Prof. Fang Liu, and Prof. Hans-Olof Andrén first of all for giving me the opportunity to enjoy an adventurous life as a PhD student. Besides, I am very grateful for having you as an unlimited source of inspiration and finally for valuable guidance, discussion, positive attitude, kindness, and support.

I would like to thank Prof. John Hald from Technical University of Denmark for his fruitful discussions and inputs to the project, and Lennart Johansson from Siemens Turbomachinery who contributed a lot to the project by providing valuable data through mechanical tests as well helpful discussions.

My sincere thank to Dr. Anders Kvist and Dr. Stefan Gustafsson for technical microscopy support and their kind attitude and sense of humor. I would like to thank Ola Löfgren for his technical support on all my Apple-related problems.

Special thanks to my dearest “microscopy” friends for the care, friendship, and all the fun we have.

My deepest and warmest appreciations go to my parents, sister and brothers for their endless care, kindness, love, and support.

Finally, I would like to thank my beloved wife for her patience and understanding for all the long working days. Thank you very much Somi for the care, support, and your endless love!

9. References

[1] "International Energy Agency," 2014. [Online]. Available: http://www.iea.org.

[2] F. Masuyama, "History of Power Plants and Progress in Heat Resistant Steels," *ISIJ Int.*, vol. 41, no. 6, pp. 612–625, 2001.

[3] F. Abe, "Development of creep-resistant steels and alloys for use in power plants," in *Structural Alloys for Power Plants*, Woodhead publishing, 2014, pp. 250–293.

[4] Y. Yin and R. Faulkner, "Physical and elastic behaviour of creep-resistant steels," in *Creep-resistant steels*, F. Abe, T.-U. Kern, and R. Viswanathan, Eds. Woodhead publishing, 2008, pp. 217–241.

[5] R. Honeycomb and P. Hancock, *Steels microstructure and properties*. Butterworth-Heinemann, 1995.

[6] F. Abe, "Strengthening mechanisms in steel for creep and creep rupture," in *Creep-resistant steels*, F. Abe, T.-U. Kern, and R. Viswanathan, Eds. Woodhead publishing, 2008, pp. 279–305.

[7] M. Taneike, F. Abe, and K. Sawada, "Creep-strengthening of steel at high temperatures using nano-sized carbonitride dispersions.," *Nature*, vol. 424, no. 6946, pp. 294–296, 2003.

[8] K. Maruyama, "Fundamental aspects of creep deformation and deformation mechanism map," in *Creep-resistant steels*, F. Abe, T.-U. Kern, and R. Viswanatan, Eds. Woodhead publishing, 2008, pp. 265–279.

[9] H. K. Danielsen and J. Hald, "Influence of Z-phase on Long-term Creep Stability of Martensitic 9 to 12 % Cr Steels," *VGB PowerTech*, vol. 5, pp. 68–73, 2009.

[10] J. Hald, "Microstructure and long-term creep properties of 9-12% Cr steels," *Int. J. Press. Vessel. Pip.*, vol. 85, no. 1–2, pp. 30–37, 2008.

[11] A. Kostka, K. G. Tak, R. J. Hellmig, Y. Estrin, and G. Eggeler, "On the contribution of carbides and micrograin boundaries to the creep strength of tempered martensite ferritic steels," *Acta Mater.*, vol. 55, no. 2, pp. 539–550, 2007.

[12] K.-H. Mayer and F. Masuyama, "The development of creep-resistant steels," in *Creep-resistant steels*, F. Abe, T.-U. Kern, and R. Viswanathan, Eds. Woodhead publishing, 2008, pp. 15–77.

[13] R. W. Swindeman, M. L. Santella, P. J. Maziasz, B. W. Roberts, and K. Coleman, "Issues in replacing Cr-Mo steels and stainless steels with 9Cr-1Mo-V steel," *Int. J. Press. Vessel. Pip.*, vol. 81, no. 6, pp. 507–512, 2004.

[14] A. Di Gianfrancesco, S. Tiberi Vipraio, and D. Vendit, "Long term microstructural evolution of 9-12% Cr steel grades for steam power generation plants," *Procedia Eng.*, vol. 55, pp. 27–35, 2013.

[15] L. Tan, X. Ren, and T. R. Allen, "Corrosion behavior of 9-12% Cr ferritic-martensitic steels in supercritical water," *Corros. Sci.*, vol. 52, no. 4, pp. 1520–1528, 2010.

[16] W. J. Quadakkers, J. Żurek, and M. Hänsel, "Effect of water vapor on high-temperature oxidation of FeCr alloys," *Jom*, vol. 61, no. 7, pp. 44–50, 2009.

[17] A. Sedriks, “Corrosion by hot gases and molten compounds,” in *Corrosion of stainless steels*, John Wiley & Sons, 1996.

[18] H. K. Danielsen and J. Hald, “On the nucleation and dissolution process of Z-phase Cr(V,Nb)N in martensitic 12%Cr steels,” *Mater. Sci. Eng. A*, vol. 505, no. 1–2, pp. 169–177, 2009.

[19] K. Sawada, H. Kushima, and K. Kimura, “Z-phase Formation during Creep and Aging in 9–12% Cr Heat Resistant Steels,” *ISIJ Int.*, vol. 46, no. 5, pp. 769–775, 2006.

[20] Y. Tanaka, “Production of creep resistant steels for turbines,” in *Creep-resistant steels*, F. Abe, T.-U. Kern, and R. Viswanathan, Eds. Woodhead publishing, 2008, pp. 174–212.

[21] D. Porter and K. Easterling, “Crystal interfaces and microstructure,” in *Phase transformation in metals and alloys*, Nelson Thrones Ltd, 1992, pp. 110–185.

[22] F. Abe, T. Horiuchi, M. Taneike, and K. Sawada, “Stabilization of martensitic microstructure in advanced 9Cr steel during creep at high temperature,” *Mater. Sci. Eng. A*, vol. 378, no. 1–2 SPEC. ISS., pp. 299–303, 2004.

[23] V. Knežević, J. Balun, G. Sauthoff, G. Inden, and A. Schneider, “Design of martensitic/ferritic heat-resistant steels for application at 650 °C with supporting thermodynamic modelling,” *Mater. Sci. Eng. A*, vol. 477, no. 1–2, pp. 334–343, 2008.

[24] M. Hättestrand and H.-O. Andrén, “Boron distribution in 9–12% chromium steels,” *Mater. Sci. Eng. A*, vol. 270, no. 1, pp. 33–37, 1999.

[25] J. S. Lee, H. Ghassemi Armaki, K. Maruyama, T. Muraki, and H. Asahi, “Causes of breakdown of creep strength in 9Cr-1.8W-0.5Mo-VNb steel,” *Mater. Sci. Eng. A*, vol. 428, no. 1–2, pp. 270–275, 2006.

[26] A. Czyrska-Filemonowicz, A. Zielińska-Lipiec, and P. J. Ennis, “Modified 9 % Cr Steels for Advanced Power Generation : Microstructure and Properties,” *J. Achiev. Mater. Manuf. Eng.*, vol. 19, no. 2, pp. 43–48, 2006.

[27] O. Prat, J. Garcia, D. Rojas, G. Sauthoff, and G. Inden, “The role of Laves phase on microstructure evolution and creep strength of novel 9%Cr heat resistant steels,” *Intermetallics*, vol. 32, pp. 362–372, 2013.

[28] A. Di Gianfrancesco, S. T. Vipraio, and D. Venditti, “Long Term Microstructural Evolution of 9-12 % Cr Steel Grades for Steam Power Generation Plants,” *Metal*, 2012.

[29] H. K. Danielsen and J. Hald, “A thermodynamic model of the Z-phase Cr(V, Nb)N,” *Calphad Comput. Coupling Phase Diagrams Thermochem.*, vol. 31, no. 4, pp. 505–514, 2007.

[30] T. Sourmail, “Precipitation in creep resistant austenitic stainless steels,” *Mater. Sci. Technol.*, vol. 17, no. 1, 2001.

[31] H. K. Danielsen, J. Hald, F. B. Grumsen, and M. A. J. Somers, “On the Crystal Structure of Z-Phase Cr (V , Nb) N,” *Metall. Mater. Trans. A*, vol. 37, no. September, pp. 2633–2640, 2006.

[32] V. Vodarek and F. Filus, “On the role of Z-phase in heat resistant steels,” in *Metal 2011: the 20th anniversary year of the International Conference on Metallurgy and Materials*, 2011, pp. 1–6.

[33] K. Sawada, H. Kushima, K. Kimura, and M. Tabuchi, “TTP Diagrams of Z Phase in 9–12% Cr Heat-Resistant Steels,” *ISIJ Int.*, vol. 47, no. 5, pp. 733–739, 2007.

[34] L. Cipolla, H. K. Danielsen, D. Venditti, P. E. Di Nunzio, J. Hald, and M. A. J. Somers, "Conversion of MX nitrides to Z-phase in a martensitic 12% Cr steel," *Acta Mater.*, vol. 58, no. 2, pp. 669–679, 2010.

[35] S. H. Ryu and J. Yu, "A new equation for the Cr equivalent in 9 to 12 pct Cr steels," *Metall. Mater. Trans. A*, vol. 29, no. 6, pp. 1573–1578, 1998.

[36] F. Liu and H.-O. Andrén, "Initial study on Z-phase strengthened 9-12% Cr steels by atom probe tomography," in *Materials for Advanced Power Engineering*, 2010, pp. 107–116.

[37] J. Goldstein, D. Newbury, D. Joy, and C. Lyman, *Scanning Electron Microscopy and X-ray Microanalysis*. Springer, 2003.

[38] D. B. Williams and C. B. Carter, *Transmission Electron Microscopy: A textbook for materials science*. Springer, 2009.

Paper I

A new 12% chromium steel strengthened by Z-phase precipitates

F Liu, M Rashidi, L Johansson, J Hald, H-O Andrén
Submitted to Scripta Materialia

Paper II

Microstructure characterization of two Z-phase strengthened 12% chromium steels

M Rashidi, F Liu, H-O Andrén

In Proc. 10th Liège Conference: Materials for Advanced Power Engineering 2014,
Eds. J Lecomte-Beckers, O Dedry, J Oakey and B Kuhn, pp. 71-80.
(electronic form only)